ChemComm

COMMUNICATION

View Article Online
View Journal | View Issue

Cite this: *Chem. Commun.*, 2024, **60**, 12405

Received 24th September 2024,
Accepted 30th September 2024

DOI: 10.1039/d4cc04954c

rsc.li/chemcomm

Electrochemically grafted gallic acid-chitosan: a metal-free *in situ* redox platform for regiospecific oligopeptide-viral spike protein interaction†

Vinoth Krishnan,[ab] Chinnaiah Sivakumar,[ab] Kannadasan Anand Babu,[c] Sevakumaran Vigneswari,[d] Rajamani Lakshminarayanan,[e] Sudhakar Natarajan[f] and Murugan Veerapandian*[ab]

Electrochemical grafting of gallic acid with chitosan (EgGC) voltammetrically deposited on a multitude of substrates exhibiting reversible oxidoreduction suitable for sensor construction is reported. A bioreceptor customized from the fragment antigen binding region of SARS-CoV-2 neutralizing antibodies immobilized on an EgGC matrix supported the selective/specific electrochemical signal transduction with respect to different viral loads (femtogram level) of SARS-CoV-2.

The emergence of severe acute respiratory syndrome coronavirus 2 (SARS-CoV-2) in late 2019 marked a global health crisis, disrupting healthcare systems, socio-economy and technology.[1–3] The reverse transcription polymerase chain reaction (RT-PCR) has emerged as a frontline tool in the diagnosis of COVID-19, however, due to its virulence, SARS-CoV-2 poses challenges in resource limited settings demanding alternative analytical platforms.[4,5] Knowhows useful for portable, user-friendly, and rapid analytical tools devised of cost-effective sensor substrates without compromising the eco-friendliness are highly advantageous for the diagnosis of emerging/remerging viral infections like COVID-19. Electrochemical biosensor systems are promising for field deployable analyses, self-operable device integration and rapid analysis of ultra-low analyte concentration.[6,7] Nevertheless, the construction of electrochemical-active materials with durable redox behaviour, compatibility toward a range of bioreceptor(s) even at multi-layer interfaces and in complex biological matrices are highly challenging. Significant materials' chemistry was studied to explore the electrochemical sensing behaviour on a disposable carbon screen printed electrode (SPE) for diagnosis of SARS-CoV-2. For instance, electrostatically interacted methylene blue (MB) with silica microspheres exhibited a selective probing of the nucleocapsid (N) and spike (S) protein of SARS-CoV-2, enabling a limit of detection (LoD) of 1 copy μL^{-1}.[8] Electrochemically adsorbed MB on graphene oxide has been demonstrated towards the peptide-based detection of spike protein (SP) with a LoD of 0.71 pg mL^{-1}.[9] A DNA-based biosensor with a dual redox signal provided from horseradish peroxidase substrate with trimethylamine anchoring H_2O_2 exhibited an fM level detection.[1] A molecularly imprinted polymer integrated thin film electrode using potassium ferri/ferro cyanide as an external redox probe was studied for nucleoprotein of COVID-19 with a LoD of 15 fM.[6] A gold nanoparticle-decorated biochip was demonstrated for the immunosensing and aptasensing of SARS-CoV-2, enabling a LoD of 7.62 fg mL^{-1} and 1.28 pg mL^{-1}, respectively.[10] A challenge in the reported studies is the fabrication of the sensor component *i.e.*, the drop-casting approach, which could influence the signal transduction, sensitivity and detection range of the biosensor system. Thus, an electrochemical grafting strategy is devised to prepare a durable sensor platform made up of biopolymer chitosan (CS) and natural product-derived phenolic acid, gallic acid (GA). This electrochemically grafted gallic acid-chitosan (EgGC) is a greener, cost-effective, and scalable redox species, offering an eco-friendly and disposable sensor platform. Immobilization of the specific probe oligopeptide associated to the conserved fragment antigen binding (F_{ab}) region of SARS-CoV-2 neutralizing antibodies can augment the capturing of SP. Until now available electrochemical biosensors are focused on equipping the N-terminal region of the ACE2 receptor or its associated DNA/peptide nucleic acid to target N- and S-proteins of SARS-CoV-2.[8] The uniqueness of the present work is to facilitate the shortest

[a] *Electrodics and Electrocatalysis Division, CSIR-Central Electrochemical Research Institute (CECRI), Karaikudi, 630 003, Tamil Nadu, India*
[b] *Academy of Scientific & Innovative Research (AcSIR), Ghaziabad-201 002, India. E-mail: vmurugan@cecri.res.in*
[c] *Anderson Clinical Genetics, Anderson Diagnostics and Labs, Chennai, Tamil Nadu, India*
[d] *Institute of Climate Adaptation and Marine Biotechnology (ICAMB), Kuala Nerus 21030, Terengganu, Malaysia*
[e] *Ocular Infections and Antimicrobials Research Group, Singapore Eye Research Institute, The Academia, 20 College Road, Discovery Tower, Singapore 169856, Singapore*
[f] *Department of Virology and Biotechnology, ICMR-National Institute for Research in Tuberculosis (NIRT), Chennai 600031, Tamil Nadu, India*

† Electronic supplementary information (ESI) available. See DOI: https://doi.org/10.1039/d4cc04954c

regiospecific oligopeptide (15 amino acid residues) as a bio-recognition element feasible for viral variants. Unlike physical coating of sensor elements, electrochemically grafted redox species could exhibit durable electron-transfer due to intertwined functional surfaces. Amplification-free direct interaction of S-proteins from oro/nasopharyngeal swap samples of positive viral loads and the external mediator-less detection approach following *in situ* electron transfer are the uniqueness of the prepared EgGC electrode. The EgGC platform enabled an efficient loading of probe oligopeptide and exerted selective binding of SP. For the real sample validation, oro/nasopharyngeal samples of SARS-CoV-2 were tested on the disposable EgGC electrodes.

CS was deposited on SPE *via* galvanostatic deposition by protonation in an aqueous acetic environment (pH 5.0). An applied potential of −1.5 V for 15 min facilitates a spontaneous electrostatic attraction of CS on SPE.[11] Subsequently, the electrochemical grafting of GA was performed using cyclic voltammetry (−0.2 to +0.9 V, scan rate of 50 mV s^{-1}) under acidic electrolyte conditions (H_2SO_4 0.05 M, pH 2.0) on CS/SPE for 25 cycles with 0.01 M of GA (Fig. S1, ESI†). The anodic peak at +0.5 V indicates the oxidation of GA, suggesting the electrografting through adsorption process. Unlike phosphate buffered saline, sulfuric acid supported electrolyte (pH 2.0) augmented better ionic conductivity for GA adsorption. Diffusion of GA from the bulk electrolyte to the interface causes deprotonation of the carboxylic group (COO^-) mediating the covalent interaction with the abundant amine groups of CS to form an amide bond. The as-electrochemically grafted GA molecule exhibits inherent redox behaviour *via* conversion of C4/C5-OH to quinone groups. Scheme 1 depicts the mechanism of electrodeposition, electrochemical grafting and photographic images of the EgGC modified carbon substrates including glassy carbon plate, carbon cloth and SPE.

Fig. 1A indicates the CV response of the EgGC electrode matrix in 0.1 M PBS (pH 7), enabling a reversible redox behaviour with an anodic peak current density j (μA cm^{-2}) of 0.73 at a peak potential of +0.55 V and cathodic j (μA cm^{-2}) of −0.134 at peak potential of +0.44 V. The effective surface coverage of EgGC is calculated to be 2.1×10^{-9} mol cm^{-2} derived using the formula $\Gamma = Q/nFA$.[12] The scan rate-dependent study of the EgGC electrode platform was further determined and the results are depicted in Fig. S2 (ESI†). Linearity fit between peak current *vs.* scan rate (0.01 to 0.09 V s^{-1}) evidenced that the EgGC modified substrate follows a surface-adsorption controlled process at the interface of electrode–electrolyte. The electrochemical reversibility and charge transfer resistance (R_{ct}) of the pristine SPE, CS/SPE and EgGC electrode platform were evaluated using 0.005 M of $K_3[Fe(CN)_6]$ and $K_4[Fe(CN)_6]$ in 0.5 M KCl solution and the results are depicted in Fig. 1B and C. The existence of electroactive species, catecholic OH groups, in the EgGC-modified SPE exhibits better current density than pristine and CS/SPE. The electrochemical impedance spectra exhibit two semi-circles due to the external redox probe (potassium ferri/ferro cyanide) at high frequency region and internal redox probe (EgGC) at the low frequency region. The fitted equivalent circuit $R(Q(R(Q(RW))))$ components include the resistance (R) and capacitance (Q) of the two semi-circles followed by the Warburg region (W). The ECSA, R_{ct}, and double layer capacitance were calculated to be 0.003 cm^2, 347 Ω, and 2.98 mF for CS/SPE and 0.008 cm^2, 208 Ω, and 1.96 mF for EgGC, respectively. From the obtained results, the electrochemical behaviour of the EgGC electrode is found to be better at the interface. To understand the electron transfer mobility of the EgGC electrode, a pH-dependent study was performed at a fixed scan rate of 0.05 V s^{-1}. As can be seen in the histogram (Fig. 1D), the EgGC electrode enabled superior current density in acidic pH conditions followed by neutral media. The peak potential is also shifted from the anodic to the cathodic region against the tested pH condition, following the $2e^-/2H^+$ transfer mechanism (Fig. S3, ESI†). To envisage the practicality of the prepared biosensor platform, a stability study was performed using the CV technique in physiological pH conditions. Fig. S3 (ESI†) denotes the retained current density at varied cycles. The surface topology and cross-sectional image of the as-prepared EgGC electrode platform were characterized using FE-SEM analysis (Fig. S4, ESI†). The EgGC surface exhibits a smooth layer in the submicron level, owing to the grafting of GA over the CS/SPE matrix. The cross-sectional thickness of the EgGC layer on SPE was calculated to be 63 μm. The

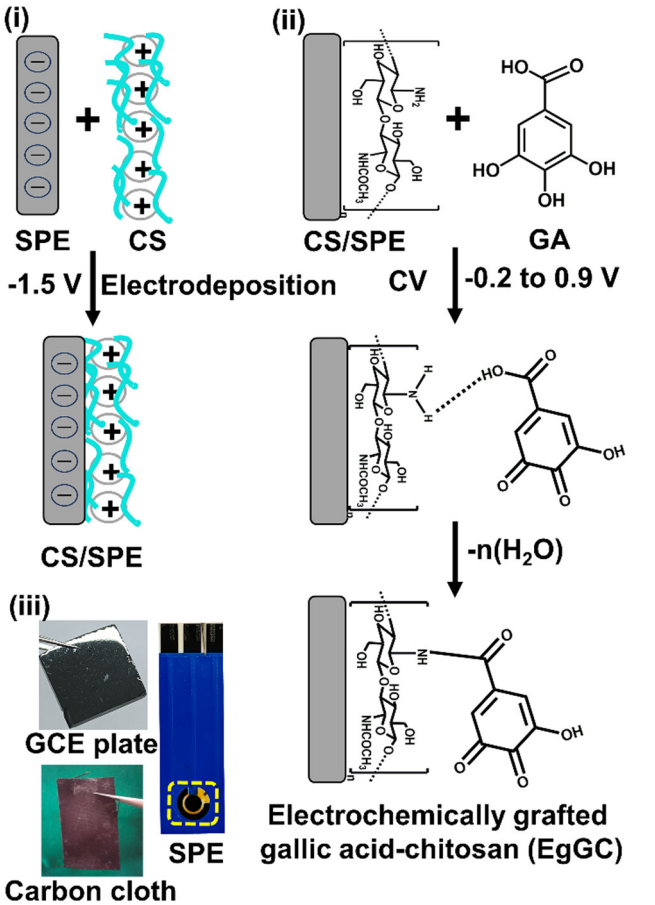

Scheme 1 (i) Electrodeposition of CS on SPE. (ii) Illustration of electrochemical grafting of GA on CS/SPE. (iii) Images of different carbon substrates coated with EgGC.

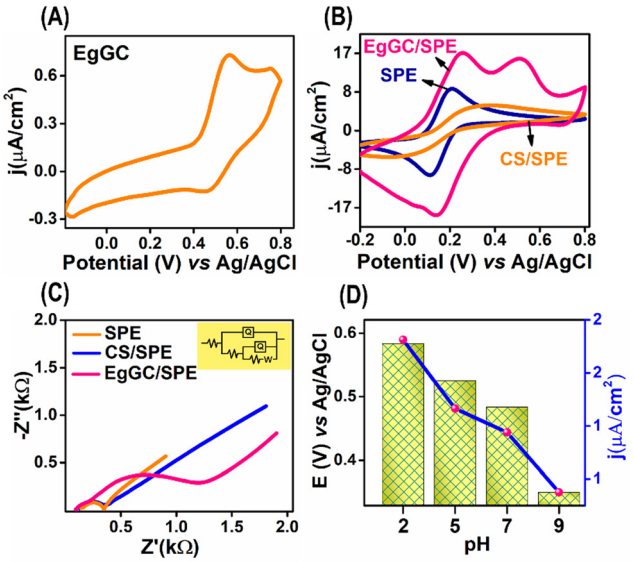

Fig. 1 (A) CV of EgGC-SPE in 0.1 M PBS (pH 7) at a scan rate of 50 mV s^{-1}. (B) CV and (C) EIS spectra of modified electrodes in 5 mM of $K_3[Fe(CN)_6]$ and $K_4[Fe(CN)_6]$ containing 0.5 M of KCl solution. (D) Histogram illustrating the pH-dependent study of the EgGC electrode platform.

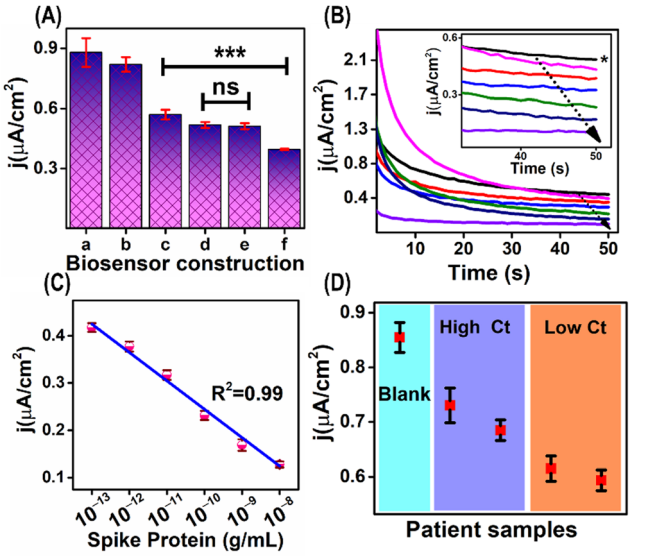

Fig. 2 (A) Histogram derived from CVs of the LBL-modified platform, (a) EgGC, (b) b-EgGC, (c) BSA-Pep/b-EgGC, (d) BSA-NP/b-EgGC, (e) SP/BSA-NP/b-EgGC, and (f) SP/BSA-Pep/b-EgGC, measured using 0.1 M PBS pH (7.4). (B) Chronoamperometry (bias potential +0.5 V) results of the EgGC biosensor platform against various concentrations of SP (100 fg mL^{-1} to 1 ng mL^{-1}) and (C) its calibration plot (*BSA-Pep/b-EgGC substrate without target sample). (D) Amperogram derived current dot plot for the two different COVID-19 positive samples tested on the BSA-Pep/b-EgGC electrode. Statistical analysis was calculated using an unpaired test with Welsh's correction (ns: statistically significant; ***$p < 0.005$).

elemental mapping not only confirmed the presence of carbon, oxygen, and nitrogen contents but also suggested the purity state of the fabricated EgGC electrode platform.

Surface chemistry and elemental composition of the GA layer on the CS/SPE surface were characterized using the XPS technique. Fig. S5 (ESI†) shows the survey spectra of the developed EgGC electrode. Fig. S6A–C (ESI†) depicts the high resolution deconvoluted spectra of the nascent and etched EgGC electrode, measured at a depth of 200 nm up to 10 layers, corroborating the elemental existence of C, O, and N species. It can be seen that after etching, the C 1s peak associated binding energy has a shift of 8 eV (286.6 eV to 278.6 eV). The O 1s peak centered at 536.8 eV is ascribed to the active oxygenated groups from GA and residues of atmospheric oxygen. Upon etching, the respective peak intensity is observed to have declining phase. Likewise, the N 1s spectra at 400.2 eV specific to the CS fragment were also analyzed before and after the etching stages. Unlike the O 1s moiety, both C 1s and N 1s related functional group peak intensities are increasing due to the etching of the grafted GA-CS (EgGC) layer. To confirm the surface chemistry between CS and GA on the electrode matrix, high-resolution C 1s, O 1s, and N 1s spectral analyses of CS/SPE and EgGC were done (Fig. S7A and B, ESI†). The deconvoluted C 1s spectra of CS/SPE exhibit three characteristic peaks at 284.5, 286, and 287 eV ascribed to the C–C, C–OH, and C–N, respectively. Compared with the CS/SPE spectrum, the C 1s of the EgGC peak related to C–N is shifted to 1.6 eV (288.6 eV), implying the N–C–O and $CONH_2$ type functionalities of hybridization. In the case of the O 1s spectra, peaks were observed for C–O (529.7 eV) and C–OH (531.5 eV) of both CS/SPE and EgGC electrodes, respectively. The N 1s spectra of CS/SPE exhibit the characteristic C–N and N–H binding energies at 398.9 and 401 eV, respectively. Upon grafting, the N 1s of EgGC exhibits an evidential signature associated with the binding energy of amide (HN–C═O) at 401.5 eV, augmenting the successful interaction between the amine groups of CS and the carbonyl moiety of GA, suggesting HN–C═O linkage during the grafting of GA onto CS.

Unlike the conventional electrochemical sensors, flexible and disposable SPE is surface-modified with EgGC for the construction of the SARS-CoV-2 biosensor platform. Schematic illustration and description on layer-by-layer fabrication of the biosensor platform is given in Fig. S8 (ESI†). Details of the custom-designed regiospecific oligopeptide (RGEMTAVFGDYWGQG) associated to the neutralizing antibodies of SARS-CoV-2 and its docking studies were given in ESI† (Table S1 and Fig. S9–S11). Histogram derived from the CV analysis after each layer modification is illustrated in Fig. 2A. To construct a biosensor platform, at first the bioaffinity layer (b) was activated on the EgGC substrate to support the immobilization of the probe oligopeptide. Subsequently, bovine serum albumin (BSA-Pep/b-EgGC) was modified to cover the unbounded sites on the b/EgGC electrode platform. To ensure the selectivity of the designed oligopeptide, negative (mismatch) oligopeptide sequence (BSA-NP/b-EgGC) was modified over the b/EgGC electrode and subjected for SP detection.

As can be seen, activation of the bioaffinity layer, bioreceptor *i.e.*, probe oligopeptide and the interaction of target SP sequentially quenches the j (μA cm^{-2}) of the EgGC electrode from 0.86 to 0.40 μA. It is worth mentioning that immobilization of the negative oligopeptide as a bioreceptor does not show sequential

variation compared to the actual probe oligopeptide, suggesting the specificity of the probe-target interaction at the electrode–electrolyte interface. Fig. 2B illustrates the chronoamperograms of the BSA-Pep/b-EgGC electrode measured against varied SP concentrations ranging from 100 fg mL^{-1} to 10 ng mL^{-1} in 0.1 M PBS (pH 7.4) as the supporting electrolyte. Upon the applied bias potential of +0.5 V in CA, concentration-dependent study shows the electrode sensitivity of 60 μA g^{-1} mL^{-1} with a coefficient determination value (R^2) of 0.99. From the calibration plot (Fig. 2C), the LoD and LoQ were calculated to be 67.6 fg mL^{-1} and 225 fg mL^{-1} using the formula LoD = 3 × σ/slope and LoQ = 10 × σ/slope, respectively. Observed CA results denote that the prepared EgGC-based oligopeptide biosensor platform is selective and sensitive towards the target SP even at ultra-low-test concentration convenient for viral disease-associated protein detection. Clinical diagnostic feasibility of the developed biosensor platform was tested using oro/nasopharyngeal swab samples of COVID-19 positive samples in comparison with RT-PCR. Real patient samples with lower cycle threshold (Ct) value indicates higher viral load and a higher Ct value indicates lower viral load. Fig. 2D and Table S2 (ESI†) demonstrate the performance of the EgGC-oligopeptide biosensor against the two different viral loads of SARS-CoV-2 samples. As can be seen, the low viral load interacted BSA-Pep/b-EgGC electrode exhibits better current density, whereas the high viral load interacted electrode exhibited impaired current density. It is worth mentioning that the test swab samples in viral transport media were directly measured on the prepared biosensor platform without isolation or amplification steps as common in RT-PCR analysis. Table S3 (ESI†) further illustrates the comparable analytical performance of the developed *in situ* redox probe biosensor without the need of additional external mediator, suggesting the user-friendly detection promising for infectious assay kit customization.

We have demonstrated the potentiality of electrochemically grafted gallic acid-chitosan as a metal-free *in situ* redox platform on disposable, flexible, glassy and fabric carbon substrates for electrochemical biosensor application. Intertwining of –COOH of GA and the $–NH_2$ group of CS augments the structural intactness at the interface enabling durable $2e^-/2H^+$ transfer reaction of catecholic OH groups of EgGC convenient for electrochemical signal transduction. Localization of the Fab regiospecific oligopeptide bioreceptor ameliorates the interaction of target SP of SARS-CoV-2, with a current sensitivity of 60 μA g^{-1} mL^{-1}, detection limit of 67.6 fg mL^{-1} and limit of quantification of 225 fg mL^{-1}. The developed redox-active sensor component could be translated for customization of other probe oligopeptide or oligonucleotide-based biomarker detection without complex pre-treatment.

This work was supported by SERB, ASEAN-India Collaborative research project (CRD/2021/000451). The authors would like to thank Dr Luke Elizabeth Hanna, Scientist 'F' and Head – Department of Virology and Biotechnology, ICMR-NIRT, Chennai for resources and laboratory support. CSIR-CECRI manuscript communication number: CECRI/PESVC/Pubs/2024-086. Authors thank the Central Instrumentation Facility Division, CSIR-CECRI for the characterization support. The study was approved by the Institutional Ethics Committee of ICMR-NIRT, Chennai, Tamil Nadu INDIA [NIRT IEC No. 2020 042].

Data availability

The data supporting this article have been included as part of the ESI.†

Conflicts of interest

The authors declare that there are no conflicts of interest.

Notes and references

1 Y. Dou, Z. Huang, T. Li, N. Maboyi, X. Ding, S. Song and J. Su, *Chem. Commun.*, 2023, **59**, 8838–8841.
2 Y. Xie, B. Bowe and Z. Al-Aly, *Nat. Commun.*, 2021, **12**, 6571.
3 M. V. F. Ferraz, E. G. Moreira, D. F. Coêlho, G. L. Wallau and R. D. Lins, *Chem. Commun.*, 2021, **57**, 6094–6097.
4 J. M. Lee, C. R. Kim, S. Kim, J. Min, M.-H. Lee and S. Lee, *Chem. Commun.*, 2021, **57**, 10222–10225.
5 H. Lukas, C. Xu, Y. Yu and W. Gao, *ACS Nano*, 2020, **14**, 16180–16193.
6 A. Raziq, A. Kidakova, R. Boroznjak, J. Reut, A. Öpik and V. Syritski, *Biosens. Bioelectron.*, 2021, **178**, 113029.
7 A. K. Yagati, T. Wu, S. G. Chavan, M.-K. Lee, M.-H. Lee and J. Min, *ACS Appl. Nano Mater.*, 2023, **6**, 17239–17250.
8 T. Chaibun, J. Puenpa, T. Ngamdee, N. Boonapatcharoen, P. Athamanolap, A. P. O'Mullane, S. Vongpunsawad, Y. Poovorawan, S. Y. Lee and B. Lertanantawong, *Nat. Commun.*, 2021, **12**, 802.
9 T. H. V. Kumar, S. Srinivasan, V. Krishnan, R. Vaidyanathan, K. A. Babu, S. Natarajan and M. Veerapandian, *Sens. Actuators, B*, 2023, **377**, 133052.
10 F. Jiang, Z. Xiao, T. Wang, J. Wang, L. Bie, L. Saleh, K. Frey, L. Zhang and J. Wang, *Chem. Commun.*, 2022, **58**, 7285–7288.
11 X. Gu, Y. Tao, Y. Pan, L. Deng, L. Bao and Y. Kong, *Anal. Chem.*, 2015, **87**, 9481–9486.
12 V. Krishnan, E. Gunasekaran, C. Prabhakaran, P. Kanagavalli, V. Ananth and M. Veerapandian, *Mater. Chem. Phys.*, 2023, **295**, 127071.

